High-resolution dynamic CE-MRA of the thorax enabled by iterative TWIST reconstruction

Jens Wetzl[1,2†], Christoph Forman[3†], Bernd J. Wintersperger[4,5], Luigia D'Errico[4,5], Michaela Schmidt[3], Boris Mailhe[6], Andreas Maier[1,2], Aurélien F. Stalder[3]

[†]These authors contributed equally to this work

Affiliations:

1 Pattern Recognition Lab, Department of Computer Science, Friedrich-Alexander-Universität Erlangen-Nürnberg, Erlangen, Germany
2 Erlangen Graduate School in Advanced Optical Technologies (SAOT), Friedrich-Alexander-Universität Erlangen-Nürnberg, Erlangen, Germany
3 Siemens Healthcare GmbH, Erlangen, Germany
4 Department of Medical Imaging, Peter Munk Cardiac Centre, Toronto General Hospital, University Health Network, Toronto, Ontario, Canada
5 Department of Medical Imaging, University of Toronto, Toronto, Ontario, Canada
6 Siemens Medical Solutions USA Inc., Princeton, USA

Correspondence to:

Jens Wetzl
Pattern Recognition Lab (Department of Computer Science)
Friedrich-Alexander-Universität Erlangen-Nürnberg
Martensstr. 3
91058 Erlangen
Germany

E-Mail: jens.wetzl@fau.de
Phone: +49 9131 85 27874
Fax: +49 9131 85 27270

Word count:

Abstract:	197	Figures:	5
Manuscript:	2800	References:	21

ABSTRACT

Purpose: To evaluate the clinical benefit of using a new iterative reconstruction technique fully integrated on a standard clinical scanner and reconstruction system using a TWIST acquisition for high-resolution dynamic 3D contrast-enhanced magnetic resonance angiography (CE-MRA).

Methods: Low-dose, high-resolution TWIST data sets of 11 patients were reconstructed using both standard GRAPPA-based reconstruction for reference and iterative reconstruction, which reduces the temporal footprint of reconstructed images. Image quality of both techniques was assessed by two experienced readers, as well as quantitatively evaluated using a time-signal curve analysis.

Results: Image quality scores consistently and significantly improved by using iterative reconstruction compared to the standard approach. Most notably, the delineation of small to mid-size vasculature improved from a mean Likert score between “non-diagnostic” and “poor” for standard to between “good” and “excellent” for iterative reconstruction. The full width at half maximum of the contrast agent bolus computed from the time-signal curve was also reduced by iterative reconstruction, allowing for more precise bolus timing.

Conclusion: Iterative reconstruction can substantially improve high-resolution dynamic CE-MRA image quality, most notably in small to mid-size vasculature. Dynamic CE-MRA with iterative reconstruction could become an alternative to conventional static 3D CE-MRA, thus simplifying the clinical workflow.

KEY WORDS

Dynamic contrast-enhanced magnetic resonance angiography; iterative reconstruction; TWIST

INTRODUCTION

Dynamic contrast-enhanced magnetic resonance angiography (dynamic CE-MRA) is performed by repeated data acquisitions typically following the intravenous injection of a Gd-based contrast agent (GBCA) (1). Today, dynamic CE-MRA techniques are widely used in clinical practice for qualitative and quantitative assessment of vascular dynamics and tissue perfusion (1). Furthermore, dynamic CE-MRA represents an improvement to the workflow of static CE-MRA by overcoming the need for bolus timing. However, dynamic CE-MRA still presents limitations regarding spatial and temporal resolution. As acquisition speed is the main limiting factor for these aspects, acceleration methods are of high interest, and parallel imaging techniques such as GRAPPA (2) are already clinically implemented for CE-MRA.

To further circumvent these limitations, techniques such as time-resolved angiography with stochastic trajectories (TWIST) (3–5) or time-resolved imaging of contrast kinetics (TRICKS) (6) update the center of k-space more frequently than its periphery and apply view-sharing for the peripheral *k*-space regions. Thus, they allow reconstructing data with high spatial resolution and fast update rates. However, such techniques suffer from relatively long temporal footprints, which may introduce temporal blurring, particularly in small vessels/edges, or might lead to reconstruction artifacts due to signal variations over long acquisition times (3,5,7).

Techniques combining sparse, incoherent sampling and iterative reconstruction were proved to be successful in accelerating MRI acquisitions in general (8), for dynamic MRI (9), static CE-MRA (10) and dynamic CE-MRA (11). Sparsity in a transform domain, e.g. the wavelet domain, allows signal recovery at sampling rates below the Nyquist sampling limit based on an ℓ_1 regularization of the coefficients in the transform domain during iterative reconstruction. For CE-MRA, sparsity by complex subtraction (12) and magnitude subtraction (11,13) in k-space has also been investigated for iterative TWIST reconstruction.

In this work, we propose an iterative reconstruction of highly accelerated, dynamic CE-MRA TWIST data with high spatial and temporal resolution on a standard clinical system. For initial evaluation of this technique, patients with suspicion or known pathologies of the chest vasculature were included. Improved signal and temporal footprint due to the novel iterative reconstruction may enable a better display of the small peripheral chest vessels with fast transit times. Therefore, we examined the potential advantages of iterative TWIST (IT-TWIST) compared to the standard reconstruction in this patient population.

METHODS

Patient Population

In this study, MRA data sets of 11 patients (age 44.6±10.7; 7 female, 4 male) undergoing clinically indicated cardiovascular MRI for assessment/confirmation of thoracic aortic pathologies (e.g. aneurysm, coarctation) were included. The study was approved by the local Research Ethics Board and the need for written informed consent was waived.

Acquisition

All data sets were acquired on a clinical 3T whole body system (MAGNETOM Skyra fit, Siemens Healthcare GmbH, Erlangen, Germany) using 30 channels (18 and 12 coil elements, respectively, of a standard body and spine array). Coverage of the thoracic aorta was ensured by a standard product TWIST technique employed in a parasagittal orientation with a slab thickness of 105.6 mm. Acquisition was performed after bolus injection of 2 ml Gadobutrol (Gadovist®, Bayer Schering Pharma, Berlin, Germany) diluted in 6 ml NaCl with an injection speed of 3 ml/s. Contrast agent dilution was performed in order to match the injection parameters of a subsequent high-resolution static 3D CE-MRA, which was timed to the thoracic aorta based on TWIST results. Patients were instructed to hold their breath after inspiration as long as they possibly can, followed by shallow breathing. The TWIST technique was acquired with interleaved series of central *k*-space regions (A) and differently and stochastically sampled peripheral *k*-space regions (B_1 to B_5), which jointly represent a regular undersampling for the given acceleration factors (cf. Figure 1, left) (3–5). Detailed acquisition parameters were as follows: repetition time: 2.89 ms; echo time: 1.05 ms; flip angle: 17°; sampling bandwidth: 570 Hz/pixel; field of view: 333 x 380 x 88 mm^3; image matrix: 269 x 384 x 73; voxel size: 1.2 x 1.0 x 1.2 mm^3 interpolated to 1 mm^3 isotropic resolution; slice oversampling: 18 %; partial Fourier: 6/8 (phase-encoding direction, PE), 7/8 (partition direction, PA); acceleration factor: 4 (PE) x 2 (PA); integrated reference scan region: 24 x 24 samples; size of the fully sampled central k-space region A: 15 %; sampling density of the peripheral k-space region B: 20 %; number of measurements (i.e. number of A-B pairs): 16-24. The acquisition durations T_A and T_B for k-space center and periphery regions were 1.2 s each, giving an acquisition time of 2.4 s per measurement and a total acquisition time of 51-73s.

Data Reconstruction

The acquired data were reconstructed with two strategies, “TWIST” and “IT-TWIST”. The TWIST reconstruction was directly performed after the acquisition. The prototype IT-TWIST reconstruction was done retrospectively, but also with the reconstruction system of the MR scanner.

As a reference, TWIST reconstruction with GRAPPA (2) was performed by combining each A region with five neighboring B regions (cf. Figure 1, left). The three B regions acquired previously to the corresponding A were used, as well as the two following it. The temporal footprint of the TWIST reconstruction was thus $4T_A + 5T_B = 10.8$ s.

For IT-TWIST, consecutive A-B pairs were reconstructed, which reduces the temporal footprint of frames to $1T_A+1T_B = 2.4$ s, but also increases undersampling (see Figure 1, right). To recover the frames $\{\hat{\boldsymbol{x}}_t\}_{t=1,\dots,T}$ for all time points T, a non-linear, iterative SENSE-type reconstruction (14) with spatio-temporal ℓ_1 wavelet regularization was performed as (15,16):

$$\{\hat{\boldsymbol{x}}_t\}_{t=1,\dots,T} = \operatorname{argmin}_{\{\boldsymbol{x}_t\}} \sum_{t=1}^{T} \left(\sum_{c=1}^{C} \| \boldsymbol{A}_t \boldsymbol{F} \boldsymbol{S}_c \boldsymbol{x}_t - \boldsymbol{y}_{t,c} \|_2^2 + \lambda_\sigma \| \boldsymbol{W}_\sigma \boldsymbol{x}_t \|_1 \right) + \lambda_\tau \| \boldsymbol{W}_\tau \left(\boldsymbol{x}_1^\top \ \cdots \ \boldsymbol{x}_T^\top \right)^\top \|_1, \quad [1]$$

where C denotes the number of coils, $\boldsymbol{A}_t$ is the sampling pattern for time t, $\boldsymbol{F}$ is the Fourier transform, $\boldsymbol{S}_c$ the multiplication by the sensitivity of coil c, $\boldsymbol{y}_{t,c}$ the measured data for time t and coil c (from an A and B region), λ_σ and λ_τ are the spatial and temporal regularization parameters and $\boldsymbol{W}_\sigma$ and $\boldsymbol{W}_\tau$ are spatial and temporal redundant Haar wavelet transforms.

To solve equation [1], the FISTA optimization (15) alternated a gradient descent step for the quadratic terms and the evaluation of the proximal operator of the ℓ_1 terms. In contrast to (15), the solution of the proximal step was computed using a memory-efficient algorithm proposed by Chambolle and Pock (17). The optimization was implemented on the graphics processing unit (GPU) to achieve clinically acceptable reconstruction times.

In order to fit all required data into limited GPU memory, the reconstruction was decoupled by performing a Fourier transform along the fully-sampled readout direction, thus reducing to many 2D+t reconstruction problems with a smaller memory requirement, which can be computed in parallel. Time-averaged coil sensitivity maps were used, which were computed similarly as ESPIRiT autocalibration (18).

The reconstruction was fully integrated on a standard clinical scanner reconstruction system (8-core 2.1 GHz Intel® Xeon® processor, 64 GB RAM, NVIDIA® Tesla™ K10 GPU with 8 GB VRAM). Unless otherwise noted, the reconstruction parameters used were 20 FISTA iterations, $\lambda_\sigma = 0.002$ and $\lambda_\tau = 5\lambda_\sigma$.

To determine appropriate parameters for the iterative reconstruction, one patient data set was reconstructed with a varying number of iterations (between 1 and 80 iterations) and regularization factors (between 0.0002 and 0.02). Convergence of the iterative process was determined by monitoring the value of the objective function in equation [1]. Visual inspection of the results for different regularization factors was used to pick an appropriate regularization value.

Clinical Image Quality Assessment

In order to evaluate the clinical impression of both applied reconstruction algorithms, two blinded readers (3 and 20 years of cardiovascular MR experience) separately evaluated the data sets using a 5-point Likert scale (0=non-diagnostic; 1=poor; 2=fair; 3=good; 4=excellent), which were presented in a random order (19). The following aspects were evaluated on all data: 1) Overall appearance of the aortic contrast-to-noise ratio (CNR) on subtracted maximum intensity projection (MIP) images, 2) Aortic delineation on peak enhancement source images (non-subtracted), 3) Overall pulmonary vasculature (mid- to small-size) delineation on subtracted MIP images (if covered by the data acquisition). All image quality related data is presented as mean ± standard deviation (median). Image quality readings between applied reconstruction algorithms were compared using Wilcoxon rank-sum tests. Statistical significance was assumed for $P < 0.05$.

Additionally, a temporal analysis was performed on all data sets to compare the time-signal curves of TWIST and IT-TWIST reconstructions after intensity normalization to ensure comparability. The analysis was performed in vascular territories of different sizes. For large

vessel representation, the ascending aorta (AAo) and main pulmonary artery (MPA) were selected. For medium and small vessel size, medial and distal aspects of the branching pulmonary artery (PA) tree as well as small and mid-size pulmonary veins (PV) were selected, respectively. Regions of interest (ROIs) in individual vessels were chosen as large as possible with respect to the vessel diameters. Typical values of ROI diameters were 47, 33, 8, 7, 2 and 3 mm, and lengths of ROIs in blood flow direction were 30, 36, 24, 23, 23 and 16 mm for MPA, AAo, medium PA, medium PV, small PA and small PV, respectively. The same ROIs were used for TWIST and IT-TWIST. For each of the resulting time-signal curves, the full width at half maximum (FWHM) was calculated to estimate the bolus sharpness.

RESULTS

Data acquisition and reconstruction were successful in all 11 cases. Reconstruction times for a dataset with 16 measurements were approximately 1:15 min and 18:30 min for the TWIST and IT-TWIST reconstruction, respectively.

The objective function value during iterative reconstruction was reduced by 99 % after 20 iterations. The remaining improvement between 20 and 80 iterations were only 0.9 %, thus indicating good convergence after 20 iterations.

The impact of changes in regularization on MIP reconstructions as well as source images is demonstrated in Figure 2. While a choice of λ_σ = 0.0002 shows good vessel delineation, noise suppression is suboptimal. In contrast, λ_σ = 0.02 leads to blurring of small vasculature. λ_σ = 0.002 was visually determined to be the best compromise between both aspects.

Clinical Image Quality Assessment

Figures 3 and 4 qualitatively show the image quality improvements between TWIST and IT-TWIST reconstructions in three representative patients with ascending aortic aneurysm, aortic root aneurysm and after aortic coarctation repair.

For the quantitative evaluation, with respect to the overall appearance of the apparent aortic contrast-to-noise, both readers rated IT-TWIST significantly higher than TWIST (Reader 1 (R1): 3.7±0.5 (median: 4) vs. 2.6±0.5 (median: 3), *P*=0.001; Reader 2 (R2): 3.5±0.7 (median: 4) vs. 2.5±0.8 (median: 2), *P*=0.002). IT-TWIST also demonstrated significant improvement of the large arterial vessel delineation as compared to TWIST (R1: 3.6±0.5 (median: 4) vs. 2.7±0.8 (median: 3), *P*=0.0039; R2: 3.6±0.5 (median: 4) vs. 2.7±0.8 (median: 3), *P*=0.0039). The overall image quality of the small to mid-size pulmonary vasculature demonstrated major improvements as assessed (n=10; in one case, no small/mid-size pulmonary vessels were covered by the aortic TWIST) by both readers (R1: 3.2±1.0 (median: 3.5) vs. 0.7±0.7 (median: 1), *P*=0.002; R2: 3.2±1.2 (median: 4) vs. 0.7±0.8 (median: 0.5), *P*=0.002). Supporting Figure S1 shows a box plot of the results, raw results are in Supporting Table S2.

Exemplary time-signal curves of one data set in large, medium and small vessels for both reconstructions are shown in Figure 5. Overall, the time-signal curves of both approaches had almost identical shapes in large vessels and similar shapes in small and mid-size vessels.

Within the large vessels (ascending aorta, main pulmonary artery), the peak signal intensity between standard and iterative reconstruction did not differ. However, small and mid-size pulmonary vessels, both arteries and veins, demonstrated substantially higher peak signal intensities with IT-TWIST as compared to TWIST. In both reconstruction approaches, the peak signal intensity dropped with decreasing vessel size. However, this effect was substantially more pronounced for TWIST reconstruction as compared to IT-TWIST, e.g. the remaining signal in a distal segment of the pulmonary artery relative to the main pulmonary artery was 50 % ± 23 % for IT-TWIST, but only 24 % ± 18 % for TWIST.

In addition, the full width at half maximum (FWHM) of contrast agent bolus signal for small vessels was substantially smaller with the iterative reconstruction (FWHM = 8.5 ± 2.9 / 10.5 ± 4.7 s for the distal pulmonary artery/pulmonary vein) than for the standard reconstruction (FWHM = 12.0 ± 7.1 / 13.6 ± 4.5 s for the distal pulmonary artery/pulmonary vein). Supporting Table S3 lists the FWHM for all vessels.

DISCUSSION

In this work, an iterative reconstruction technique for standard dynamic 3D CE-MRA TWIST data was integrated on a routine clinical scanner and evaluated in 11 patients. Presented results demonstrate the overall improvement in image quality using iterative approaches for reconstruction of high-resolution TWIST data. The marked improvement of small pulmonary vasculature delineation and the demonstrated improvement of vascular contrast agent kinetics are the most important findings of this preliminary study.

Using IT-TWIST, the diagnostic value of the data sets was consistently improved. For the aorta, the overall appearance of the MIP images as well as the vessel delineation of the source images had a mean score between “fair” and “good” for the TWIST reconstruction, indicating diagnostic image quality. However, using IT-TWIST with the same data, the scores increased by about one level, to between “good” and “excellent”. For the pulmonary vasculature delineation, the scores averaged between “non-diagnostic” and “poor” using TWIST. Using IT-TWIST, the scores of the pulmonary vasculature significantly increased to the range “good” to “excellent”. This remarkable improvement indicates that the pulmonary vasculature that was not visible using the standard reconstruction is now visible using iterative reconstruction (cf. also Figures 3, 4). For pulmonary vasculature delineation, the lowest score given for IT-TWIST was “poor” in two cases. However, these cases had a score of “non-diagnostic” using standard TWIST reconstruction, so iterative reconstruction was still an improvement. The lower score using both reconstruction techniques for these data sets may be due to the apparent breathing motion at the end of the acquisition. It may be possible to improve this aspect in an iterative reconstruction also addressing respiratory motion during optimization (20,21). Our results also agree with a previously reported reduction in temporal footprint using iterative reconstruction (11). In one representative data set, the FWHM of the bolus peak in a small pulmonary artery/vein was reduced from 12.0 / 14.2 s to 10.1 / 12.0 s. This indicates a sharper apparent contrast agent bolus, a shorter temporal footprint and less temporal blurring. It can be hypothesized that the combination of a shorter temporal footprint together with the improvements due to iterative reconstruction itself are responsible for the important image quality gains. This is particularly

observable in regions with short bolus transit times and small vessel diameters, such as in the small pulmonary vasculature.

These preliminary results suggest that it might be possible to improve dynamic CE-MRA of smaller vascular regions, such as the pulmonary vasculature.

The TWIST data in this study were acquired with a low dose of contrast agent (for the purpose of bolus timing), because it was followed by a conventional high-resolution 3D CE-MRA acquisition. The good to excellent depiction of the pulmonary vasculature with such a low dose indicates the potential of the technique for low dose applications. Alternatively, it might be possible to reach even better image quality by using a relatively higher dose of contrast agent. However, this would require further detailed investigation. A higher dose and longer injection times may have resulted in better image quality using the TWIST reconstruction. Nonetheless this would result in an increased temporal overlap of arterial and venous phases.

The idea of using conventional TWIST data, which are intrinsically incoherent, with iterative reconstruction has been suggested previously (11). Beyond differences in the iterative reconstruction techniques, our reconstruction technique was integrated on a standard clinical system. Using a clinically available reconstruction system with a GPU, it was possible to substantially reduce the reconstruction times to less than 20 minutes, despite the large matrix sizes. The inline integration together with shorter reconstruction times may contribute to a wider clinical acceptance of iterative reconstruction techniques.

In this work, we demonstrated superior image quality at high acceleration factors using iterative reconstruction. The resulting data thus feature higher spatial and temporal resolution in comparison to typical TWIST protocols. Considering the high image quality with the current acceleration level, it might be possible to achieve even higher acceleration and spatial/temporal resolution with clinically acceptable image quality. It may eventually be possible to perform dynamic 3D CE-MRA with the resolution of current high-resolution 3D CE-MRA. This may improve the diagnostic value in pathologies like arteriovenous malformations, where high temporal resolution is essential. Furthermore, high-resolution dynamic 3D CE-MRA would present a substantially simpler workflow compared to conventional static 3D CE-MRA acquisitions.

The regularization used in this work was based on evaluations performed in one dataset. While the results indicate a consistent image quality over all the patients, a dependency of this parameter on the datasets was not evaluated.

The selected TWIST imaging protocol was optimized for temporal and spatial resolution, and, as such, a better image quality for large vessels could have been achieved with lower acceleration for standard TWIST reconstruction. However, this would have also resulted in lower temporal and spatial resolution, further impairing small vessel delineation.

Despite the fact that image data reading was performed in a blinded fashion with random presentation of image data, readers may have been able to identify the underlying type of reconstruction based on the obviously different image appearance of iterative algorithms. The

very similar, sometimes identical, scores both readers gave within each category may be due to the discrete 5-point Likert scale which was used and the high precision of the readers.

While the use of the proposed GPU based algorithm allowed for substantial reduction in reconstruction times, reconstruction times greater than 10 minutes remain challenging in a clinical setting. Nevertheless, based on the scalability of the proposed algorithms, further speedup of reconstruction performance is expected using more GPUs.

CONCLUSION

We have presented a preliminary study demonstrating the benefits of iterative reconstruction for dynamic 3D CE-MRA. In particular, small vessel delineation was markedly improved, thus suggesting an alternative to the currently used high-resolution static CE-MRA for imaging smaller vasculature. Our results demonstrate that such high image quality can be achieved even with a low dose of contrast agent. The implementation of the reconstruction algorithm on standard scanner hardware using GPU acceleration enables the use of iterative reconstruction in clinical practice, warrants future larger clinical studies and may eventually contribute to a wider acceptance of CE-MRA.

ACKNOWLEDGEMENTS

The authors gratefully acknowledge funding of the Erlangen Graduate School in Advanced Optical Technologies (SAOT) by the German Research Foundation (DFG) in the framework of the German excellence initiative.

REFERENCES

1. Hadizadeh DR, Marx C, Gieseke J, Schild HH, Willinek WA. High temporal and high spatial resolution MR angiography (4D-MRA). Rofo 2014;186:847–59. doi: 10.1055/s-0034-1366661.

2. Griswold MA, Jakob PM, Heidemann RM, Nittka M, Jellus V, Wang J, Kiefer B, Haase A. Generalized autocalibrating partially parallel acquisitions (GRAPPA). Magn. Reson. Med. 2002;47:1202–10. doi: 10.1002/mrm.10171.

3. Lim RP, Shapiro M, Wang EY, et al. 3D time-resolved MR angiography (MRA) of the carotid arteries with time-resolved imaging with stochastic trajectories: comparison with 3D contrast-enhanced Bolus-Chase MRA and 3D time-of-flight MRA. AJNR. Am. J. Neuroradiol. 2008;29:1847–54. doi: 10.3174/ajnr.A1252.

4. Nael K, Krishnam M, Ruehm SG, Michaely HJ, Laub G, Finn JP. Time-resolved MR angiography in the evaluation of central thoracic venous occlusive disease. AJR. Am. J. Roentgenol. 2009;192:1731–8. doi: 10.2214/AJR.08.1919.

5. Song T, Laine AF, Chen Q, Rusinek H, Bokacheva L, Lim RP, Laub G, Kroeker R, Lee VS. Optimal k-space sampling for dynamic contrast-enhanced MRI with an application to MR renography. Magn. Reson. Med. 2009;61:1242–8. doi: 10.1002/mrm.21901.

6. Korosec FR, Frayne R, Grist TM, Mistretta CA. Time-resolved contrast-enhanced 3D MR angiography. Magn. Reson. Med. 1996;36:345–51.

7. Steeden JA, Pandya B, Tann O, Muthurangu V. Free breathing contrast-enhanced time-resolved magnetic resonance angiography in pediatric and adult congenital heart disease. J. Cardiovasc. Magn. Reson. 2015;17:38. doi: 10.1186/s12968-015-0138-9.

8. Lustig M, Donoho D, Pauly JM. Sparse MRI: The application of compressed sensing for rapid MR imaging. Magn. Reson. Med. 2007;58:1182–95. doi: 10.1002/mrm.21391.

9. Gamper U, Boesiger P, Kozerke S. Compressed sensing in dynamic MRI. Magn. Reson. Med. 2008. doi: 10.1002/mrm.21477.

10. Stalder AF, Schmidt M, Quick HH, Schlamann M, Maderwald S, Schmitt P, Wang Q, Nadar MS, Zenge MO. Highly undersampled contrast-enhanced MRA with iterative reconstruction: Integration in a clinical setting. Magn. Reson. Med. 2014. doi: 10.1002/mrm.25565.

11. Rapacchi S, Natsuaki Y, Plotnik A, Gabriel S, Laub G, Finn JP, Hu P. Reducing view-sharing using compressed sensing in time-resolved contrast-enhanced magnetic resonance angiography. Magn. Reson. Med. 2014. doi: 10.1002/mrm.25414.

12. Trzasko JD, Haider CR, Borisch EA, Campeau NG, Glockner JF, Riederer SJ, Manduca A. Sparse-CAPR: highly accelerated 4D CE-MRA with parallel imaging and nonconvex compressive sensing. Magn. Reson. Med. 2011;66:1019–32. doi: 10.1002/mrm.22892.

13. Rapacchi S, Han F, Natsuaki Y, Kroeker R, Plotnik A, Lehrman E, Sayre J, Laub G, Finn JP, Hu P. High spatial and temporal resolution dynamic contrast-enhanced magnetic resonance

angiography using compressed sensing with magnitude image subtraction. Magn. Reson. Med. 2014;71:1771–83. doi: 10.1002/mrm.24842.

14. Pruessmann KP, Weiger M, Scheidegger MB, Boesiger P. SENSE: sensitivity encoding for fast MRI. Magn. Reson. Med. 1999;42:952–62.

15. Liu J, Rapin J, Chang T, Lefebvre A, Zenge M, Mueller E, Nadar MS. Dynamic cardiac MRI reconstruction with weighted redundant Haar wavelets. In: Proc. Intl. Soc. Mag. Reson. Med. 20. ; 2012. p. 178.

16. Wetzl J, Schmidt M, Zenge M, Lugauer F, Lazar L, Nadar MS, Maier A, Hornegger J, Forman C. Isotropic 3-D CINE Imaging with Sub-2mm Resolution in a Single Breath-Hold. In: Proc. Intl. Soc. Mag. Reson. Med. 23. ; 2015. p. 1011.

17. Chambolle A, Pock T. A First-Order Primal-Dual Algorithm for Convex Problems with Applications to Imaging. J. Math. Imaging Vis. 2010;40:120–145.

18. Uecker M, Lai P, Murphy MJ, Virtue P, Elad M, Pauly JM, Vasanawala SS, Lustig M. ESPIRiT - an eigenvalue approach to autocalibrating parallel MRI: where SENSE meets GRAPPA. Magn. Reson. Med. 2014;71:990–1001.

19. Likert R. A technique for the measurement of attitudes. Arch. Psychol. 1932;22:55.

20. Cheng JY, Zhang T, Ruangwattanapaisarn N, Alley MT, Uecker M, Pauly JM, Lustig M, Vasanawala SS. Free-breathing pediatric MRI with nonrigid motion correction and acceleration. J. Magn. Reson. Imaging 2014;42:407–20. doi: 10.1002/jmri.24785.

21. Forman C, Grimm R, Hutter J, Maier A, Hornegger J, Zenge MO. Free-Breathing Whole-Heart Coronary MRA: Motion Compensation Integrated into 3D Cartesian Compressed Sensing Reconstruction. In: Mori K, Sakuma I, Sato Y, Barillot C, Navab N, editors. MICCAI 2013, Part II, LNCS 8150. Berlin Heidelberg; 2013. pp. 575–582.

FIGURES

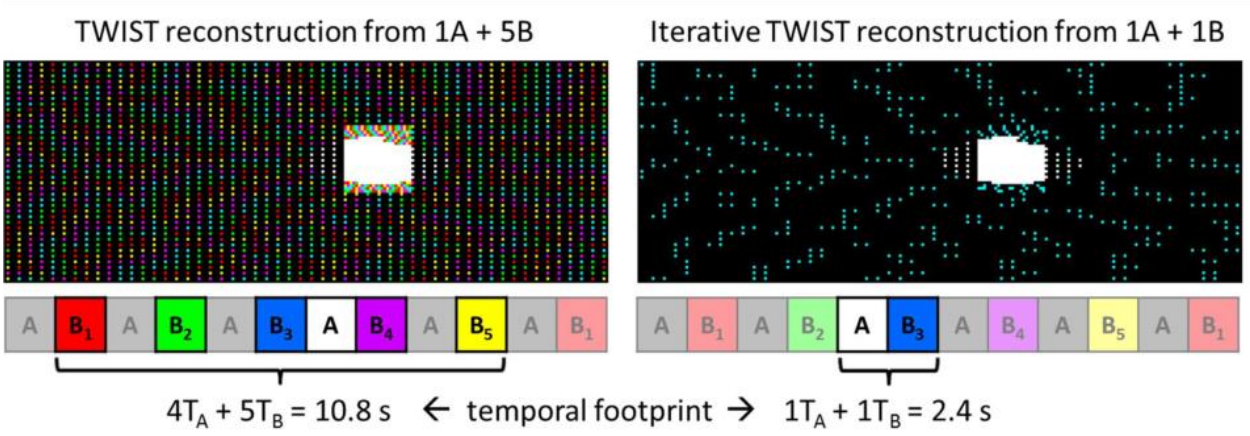

Figure 1. The TWIST acquisition repeats the series of sampling patterns: A-B_1-A-B_2-A-B_3-A-B_4-A-B_5, each B region corresponding to different k-space positions (visualized as different colors above), that, when combined, form a full regularly undersampled k-space periphery. The TWIST reconstruction uses a single A and the five closest B regions to obtain a k-space suitable for GRAPPA reconstruction (left). Our proposed iterative TWIST reconstruction uses only a single A-B pair, thus minimizing its temporal footprint (right).

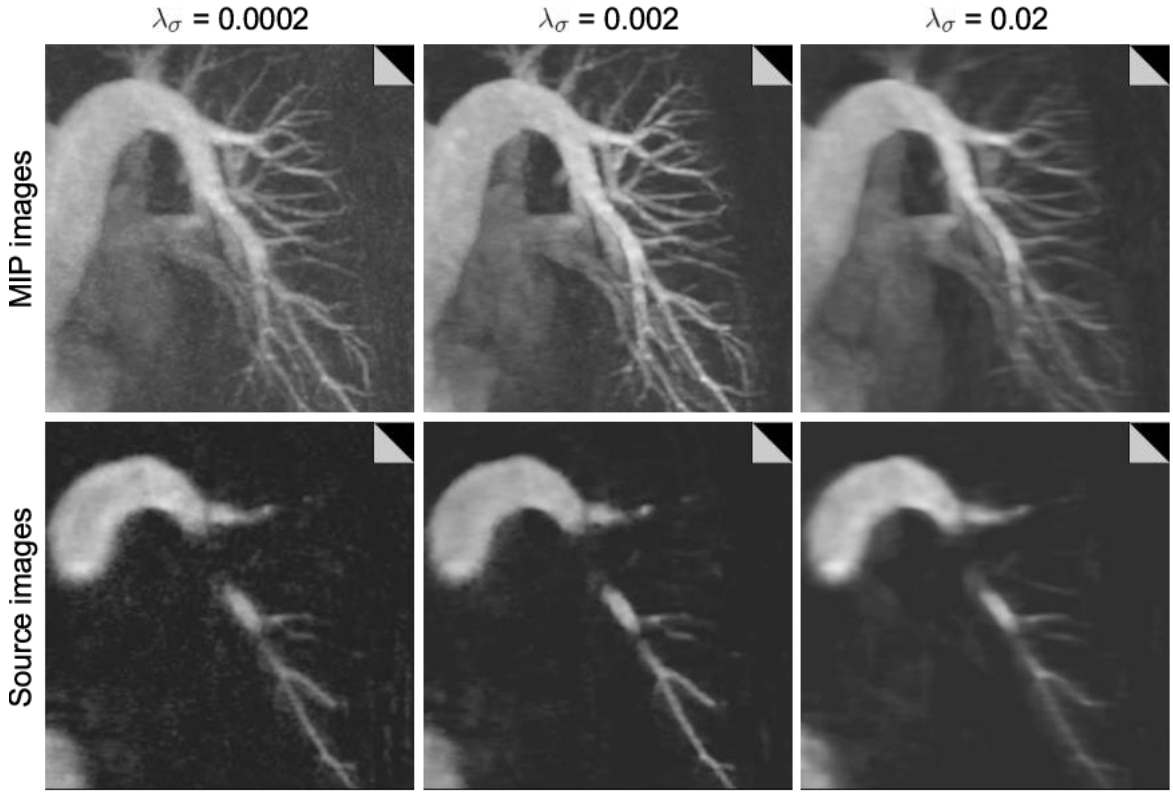

Figure 2. MIP and source images of IT-TWIST reconstructions with different regularization parameters. The parameter λ_σ = 0.002 was chosen as the best compromise for vessel delineation vs. noise.

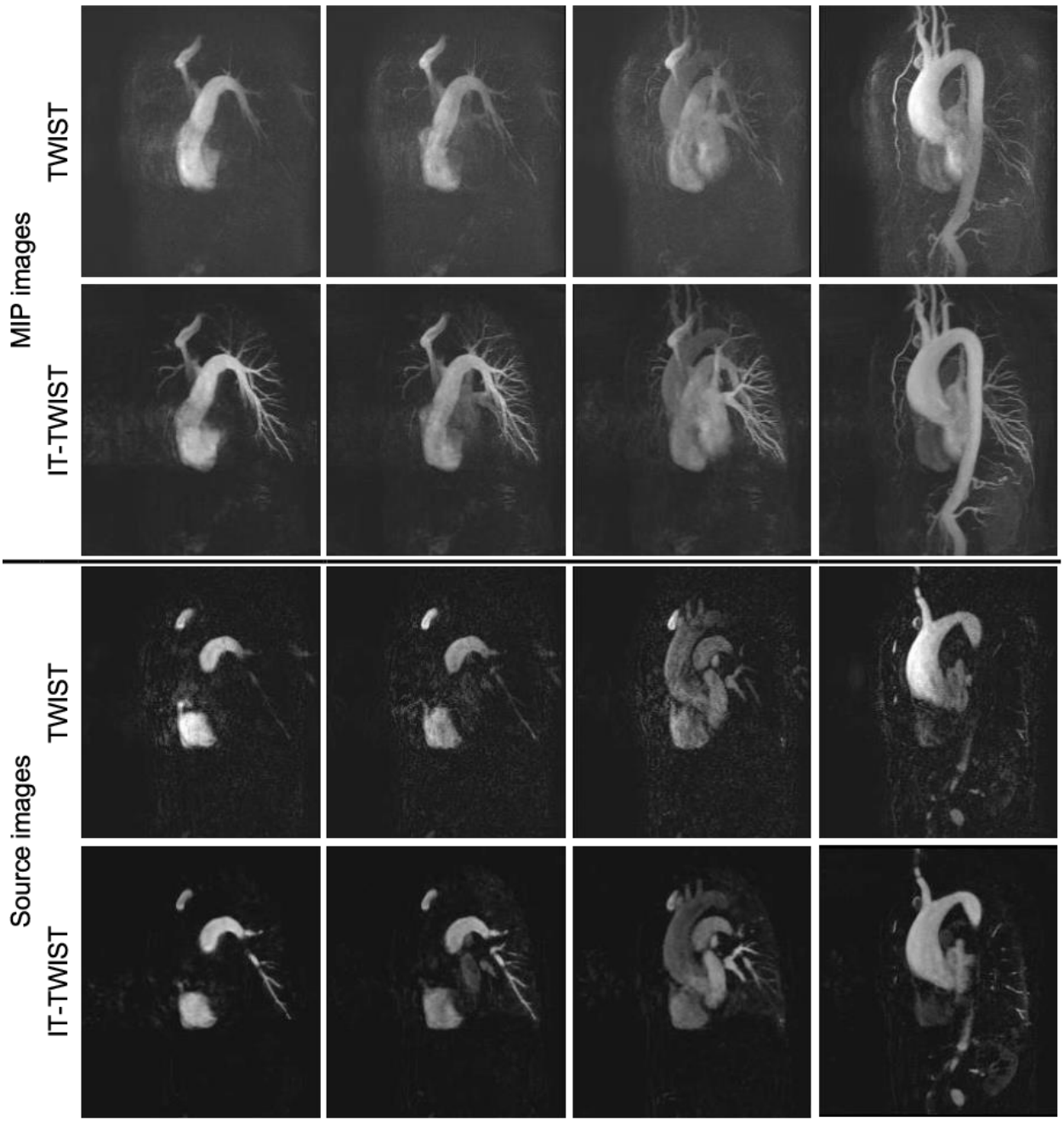

Figure 3. Subtracted MIP and corresponding slices of source images over time (columns) from standard TWIST and IT-TWIST reconstructions in a patient with known ascending aortic aneurysm. Comparison of the MIP images shows the substantially better delineation of small to mid-size pulmonary vasculature, which can also be seen in the corresponding source images.

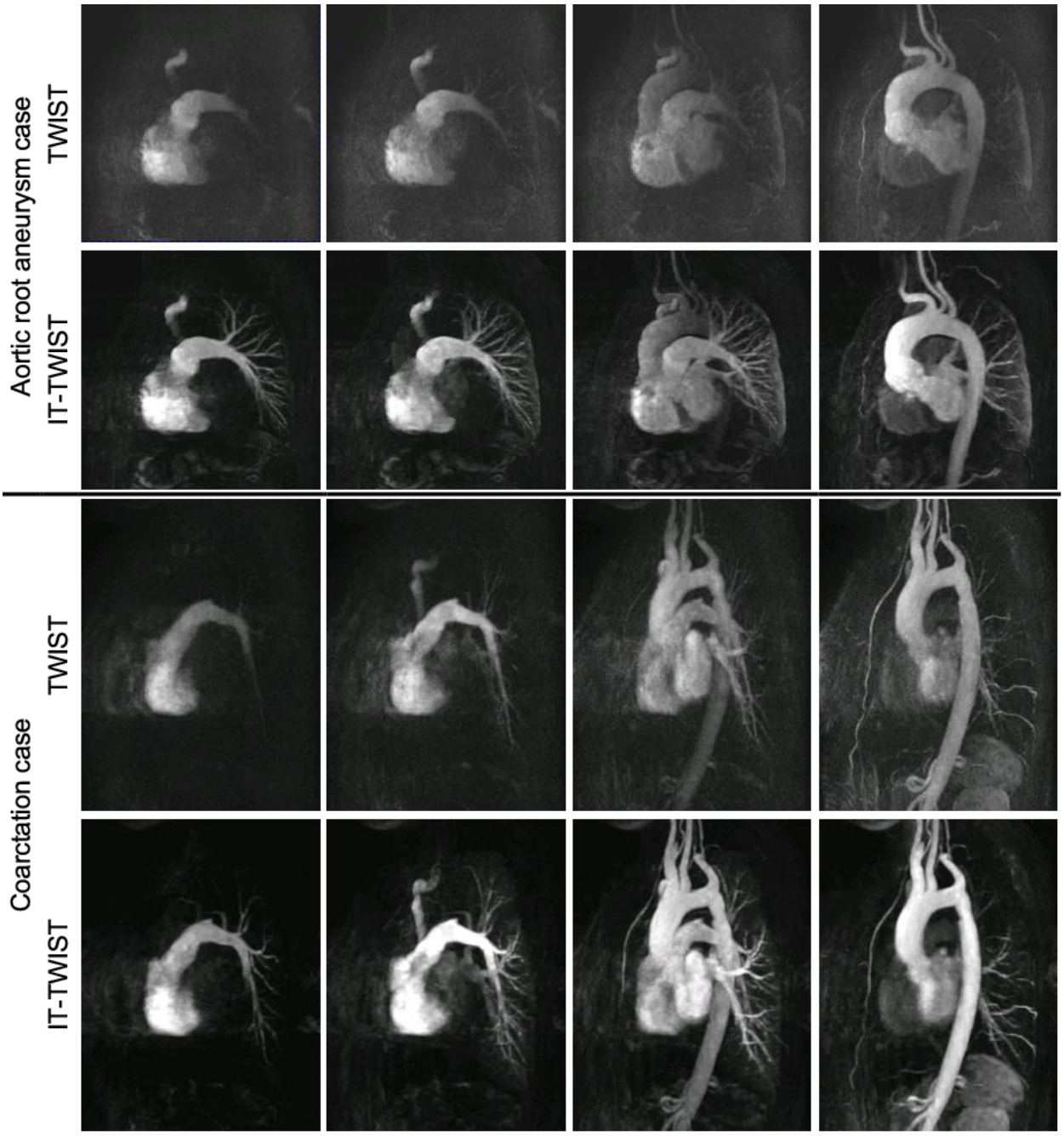

Figure 4. Subtracted MIP images over time (columns) of patients with aortic root aneurysm (top rows) and after aortic coarctation repair (bottom rows). Both cases show marked improvement of the apparent CNR and pulmonary vasculature delineation, with parenchymal enhancement displayed in the upper case.

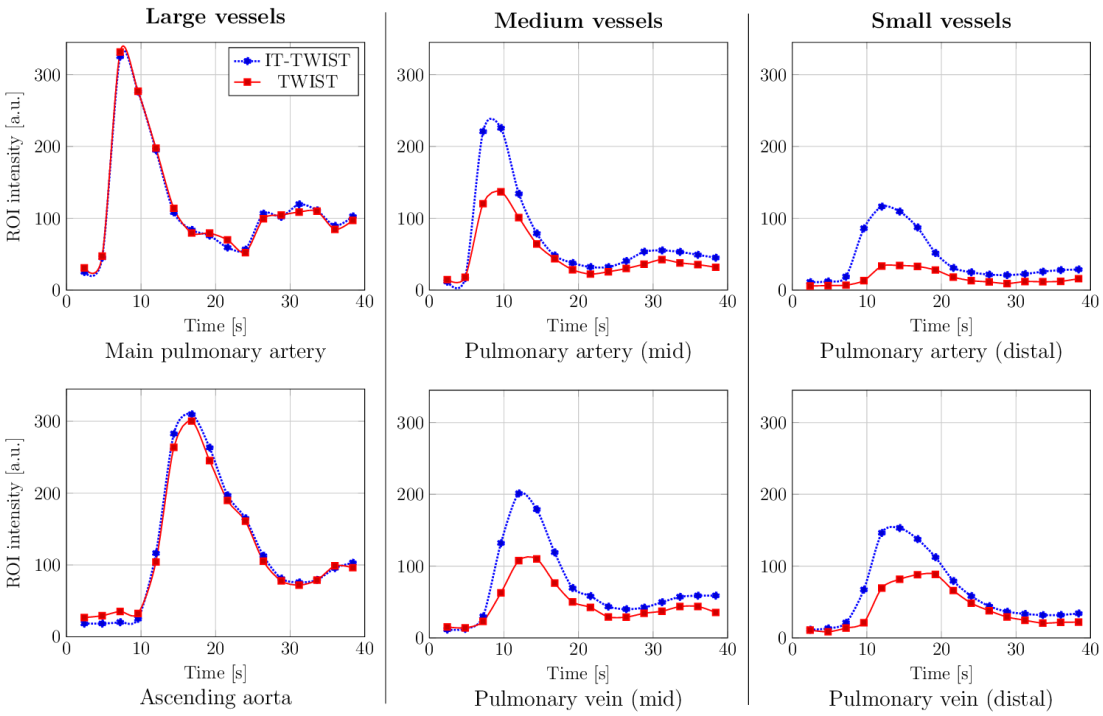

Figure 5. ROI time-signal curve analysis: TWIST (red line with squares) vs. IT-TWIST (blue, dotted line with circles) reconstructions in the patient shown in Figure 3 for large, medium and small vessels. While both methods show identical performance within large vessels (main pulmonary artery, ascending aorta), IT-TWIST demonstrates a gain in peak signal intensity during the GBCA first pass in mid-size and small vasculature (mid and distal pulmonary artery/vein).

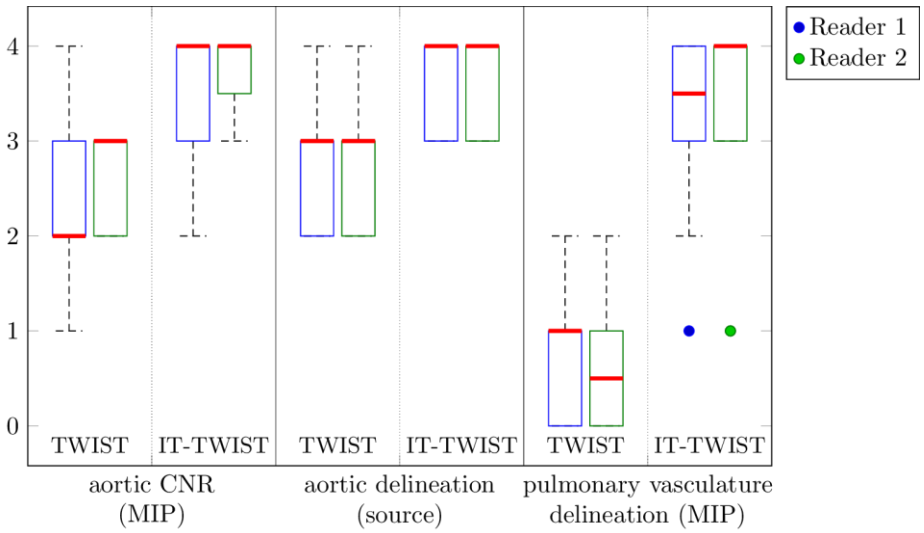

Supporting Figure S1. Box plot of the scores given by both readers for the aspects of aortic contrast-to-noise ratio, aortic delineation and pulmonary vasculature delineation. The red lines represent the median values, closed boxes show the 25 % and 75 % quantiles and dashed lines show the minimum and maximum value. The two outliers for pulmonary vasculature delineation using IT-TWIST reconstruction are marked by circles.

#	Aortic CNR (MIP)				Aortic delineation (source)				Pulm. Vasc. Delineation (MIP)			
	TWIST		IT-TWIST		TWIST		IT-TWIST		TWIST		IT-TWIST	
	R1	R2	R1	R2	R1	R2	R1	R2	R1	R2	R1	R2
1	2	2	3	3	2	2	3	3	0	0	2	1
2	3	3	4	4	3	3	4	4	1	1	4	4
3	2	2	3	4	3	3	4	4	n/a	n/a	n/a	n/a
4	3	3	4	4	4	3	4	4	1	1	4	3
5	1	2	2	3	2	2	3	3	0	0	1	1
6	2	3	4	4	2	2	4	4	1	0	4	4
7	4	3	4	4	4	4	4	4	2	2	3	4
8	2	2	3	4	2	2	3	3	0	0	4	4
9	3	3	4	4	3	3	4	4	1	2	4	4
10	2	2	3	3	2	2	3	3	0	0	3	3
11	3	3	4	4	3	4	4	4	1	1	3	4
Mean	2,5	2,5	3,5	3,7	2,7	2,7	3,6	3,6	0,7	0,7	3,2	3,2
Std.dev.	0,8	0,5	0,7	0,5	0,8	0,8	0,5	0,5	0,7	0,8	1,0	1,2
Median	2	3	4	4	3	3	4	4	1	0,5	3,5	4

Supporting Table S2. Raw Likert scores of both readers regarding the aspects of aortic contrast-to-noise ratio, aortic delineation and pulmonary vasculature delineation. In case 3, no small/mid-size pulmonary vessels were covered by the aortic TWIST.

Vessel	**FWHM [s]**	
	TWIST	**IT-TWIST**
Main pulmonary artery	7.1 ± 1.2	7.1 ± 1.4
Pulmonary artery (mid)	8.1 ± 1.7	7.1 ± 1.3
Pulmonary artery (distal)	12.0 ± 7.1	8.5 ± 2.9
Ascending aorta	10.7 ± 2.3	10.2 ± 2.4
Pulmonary vein (mid)	12.7 ± 7.2	11.5 ± 5.9
Pulmonary vein (distal)	13.6 ± 4.5	10.5 ± 4.7

Supporting Table S3. Mean and standard deviation over all cases of full width at half maximum (FWHM) of contrast agent bolus signal of different vessels for TWIST and IT-TWIST reconstruction.